Intermetallics 105 (2019) 39–43

Contents lists available at ScienceDirect

Intermetallics

journal homepage: www.elsevier.com/locate/intermet

Difference in physical properties of MAX-phase compounds Cr_2GaC and Cr_2GaN induced by an anomalous structure change in Cr_2GaN

Haiyun Tong[a,b], Shuai Lin[a,*], Yanan Huang[a], Peng Tong[a,**], Wenhai Song[a], Yuping Sun[c,a,d]

[a] Key Laboratory of Materials Physics, Institute of Solid State Physics, Hefei Institute of Physical Science, Chinese Academy of Sciences, Hefei, 230031, People's Republic of China
[b] University of Science and Technology of China, Hefei, 230026, People's Republic of China
[c] High Magnetic Field Laboratory, Chinese Academy of Sciences, Hefei, 230031, People's Republic of China
[d] Collaborative Innovation Center of Advanced Microstructures, Nanjing University, Nanjing, 210093, People's Republic of China

ARTICLE INFO

Keywords:
MAX-phase compound
Anomalous structure change
Electrical/thermal transport properties
Spin-density-wave
Microtopography

ABSTRACT

MAX-phase compounds with layered structure have been investigated extensively due to their excellent metallic and ceramic properties. Among them, Cr_2GaC and Cr_2GaN possess the same crystal structure and similar electronic structure, whereas Cr_2GaN undergoes a spin-density-wave transition around 170 K but Cr_2GaC is Pauli paramagnetism without any magnetic transition. To understand what make these happen, we studied the crystal structure between 300 and 35 K for both Cr_2GaC and Cr_2GaN. As the temperature decreases, the lattice constants (both a and c) decline monotonically in Cr_2GaC, while an abnormal negative thermal expansion of c axis was observed below 170 K in Cr_2GaN. The increase of c/a induced by abnormal increase of c leads to the enhancement of localization of Cr_2N plane and causes more Cr-3d electrons confinement in Cr_2N plane of Cr_2GaN. This further facilitates the reconstruction of density of states near the Fermi surface and even forms the Fermi surface nesting, resulting in the spin-density-wave transition as well as the abrupt changes of resistivity, specific heat, and density of carriers around 170 K in Cr_2GaN.

1. Introduction

The MAX-phase compounds with a general chemical formula $M_{n+1}AX_n$ (n = 1, 2, or 3; M is an early transition metal; A is a main group element; X is C or/and N) have a hexagonal structure with space group $P6_3/mmc$ (No.194) [1]. The stacking $M_{n+1}X_n$ and A layers one by one along the c axis is the feature of layered structure of MAX-phase compounds. Recently, these layered MAX-phase compounds have been studied extensively because of their unique combination of metallic (excellent electrical and thermal conductivities, high elastic modulus, as well as good machinability) and ceramic-like properties (strong oxidation and corrosion resistance) [2–10]. However, magnetically ordered states are rarely reported in MAX-phase compounds.

Among all of MAX-phase compounds, Cr-based materials ($Cr_{n+1}AX_n$) are likely to be magnetic. Although Cr_2AlC, Cr_2GaC, and Cr_2GeC are Pauli paramagnetism [11], magnetic order (ferromagnetic or ferrimagnetic order) can be introduced by magnetic elements doping in $Cr_{2-x}Mn_xAlC$ [12], $Cr_{2-x}Mn_xGaC$ [13], and $Cr_{2-x}Mn_xGeC$ [14,15]. Surprisingly, Cr_2GaN itself shows a magnetic order state of spin-density-wave (SDW) below 170 K without any magnetic elements doping [16]. Cr_2GaC and Cr_2GaN possesses the same crystal structure (Cr_2AlC-type structure), close lattice constant ($a = b = 2.894$ Å, $c = 12.615$ Å for Cr_2GaC; $a = b = 2.883$ Å, $c = 12.753$ Å for Cr_2GaN), and similar electronic structure, while Cr_2GaN shows the SDW transition and Cr_2GaCIS Pauli paramagnetism [13,16–19]. To understand the origin of SDW transition of Cr_2GaN, some theoretical and experimental works have been carried out. Z. Liu et al. proposed that the SDW transition of Cr_2GaN may be due to the Fermi surface nesting based on the analysis of electronic structure [16]. However, what induces the formation of Fermi surface nesting is not clear. Y. F. Li et al. reported that the SDW transition of Cr_2GaN can be suppressed by Ge doping, suggesting that the structure change may influence the SDW [20]. On the other hand, as mentioned above, there exists an obvious difference in magnetic property between Cr_2GaC and Cr_2GaN [16]. However, whether there are differences in other physical properties such as microtopography, resistivity, specific heat, and density of carriers is not clear.

In this paper, to explore the inducement of SDW in Cr_2GaN, we systemically investigate the change of crystal structure near the

* Corresponding author.
** Corresponding author.
E-mail addresses: linshuai17@issp.ac.cn (S. Lin), tongpeng@issp.ac.cn (P. Tong).

https://doi.org/10.1016/j.intermet.2018.11.008
Received 9 October 2018; Received in revised form 8 November 2018; Accepted 11 November 2018

temperature of SDW transition. For comparison, the crystal structure of Cr_2GaC was also carried out. Interestingly, there exists an anomalous structure change in Cr_2GaN near the SDW transition temperature. Moreover, considerable differences in microtopography, resistivity, specific heat, and density of carriers between Cr_2GaC and Cr_2GaN are reported. The anomalous structure change in Cr_2GaN is the major factor that causes the above differences.

2. Experimental details

The polycrystalline Cr_2GaC and Cr_2GaN were prepared by a solid-state reaction according to previous reports [13,16,17]. The raw materials are as follows: Cr_2N powder (2.5N, −200mesh, CW-nano Co., Ltd), Cr powder (4N, −200mesh, Alfa Aesar), graphite powder (3N, −325mesh, Sinopharm Chemical Reagent Co., Ltd), and Ga ingot (5N, Sinopharm Chemical Reagent Co., Ltd). The sketch map of crystal structure of Cr_2GaC/N was plotted by using VESTA visualization software [21]. X-ray powder diffraction (XRD) was performed using a Philips X'pert PRO X-ray diffractometer with Cu K_α radiation ($\lambda = 0.15406$ nm) from 300 to 35 K. The Rietveld refinement of XRD data was carried out by using the Rietica software. The surface and cross-sectional microtopographies as well as the compositions of our samples were determined by Field emission scanning electron microscope (FE-SEM, Quanta 200 FEG) and Energy-dispersive X-ray spectroscopy (EDX, Oxford EDX, with INCA software), respectively. The electrical transport, specific heat, Hall coefficient measurements were performed on a Quantum Design physical property measurement system (PPMS-9T).

3. Results and discussion

Fig. 1(a) presents the schematic diagram of crystal structure of Cr_2GaC/N with hexagonal symmetry (space group: $P6_3/mmc$). As shown in Fig. 1(a), Cr_2GaC and Cr_2GaN have an obvious layered structure with edge-sharing octahedral layer Cr_6C/N and Ga layer stacking level-by-level along the c axis. The dashed line portion stands for the unit cell of Cr_2GaC/N. Fig. 1(b) and (c) show the Rietveld refined room-temperature powder XRD pattern for our samples Cr_2GaC and Cr_2GaN, respectively. There is no observable diffraction patterns of impurity phases and the fitting parameters of both refinements are very low, suggesting our samples are single phase. The refined lattice constants of Cr_2GaC and Cr_2GaN ($a = b = 2.894(1)$ Å, $c = 12.615(2)$ Å for Cr_2GaC; $a = b = 2.874(1)$ Å, $c = 12.756(1)$ Å for Cr_2GaN) are very close to the corresponding values reported previously [13,16,20]. Moreover, the lattice constants of Cr_2GaC and Cr_2GaN are close to each other. Fig. 1(d) displays the surface SEM picture of Cr_2GaC bulk, and dense surface can be easily found. The inset of Fig. 1(d) shows the cross-sectional SEM micrograph of Cr_2GaC and layered microstrucutre are observed, which is consistent with the layered crystal structure of Cr_2GaC (to see Fig. 1(a)). Similarly, we also performed the measurements of SEM for Cr_2GaN, and the measured results are shown in Fig. 1(f). A few small pores are observed in surface micrograph of Cr_2GaN, and the compactness of Cr_2GaN is less than that of Cr_2GaC. As we know, the compactness of MAX-phase compounds is close related to the synthesis temperature [22]. The synthesis temperature (1000 °C) of Cr_2GaC is much higher than that of Cr_2GaN (740 °C). It is reasonable that the compactness of Cr_2GaC is better than that of Cr_2GaN. Since Cr_2GaN decomposes above 910 °C, the reaction temperature can only achieve at 740 °C [16,20]. The cross-sectional SEM micrograph of Cr_2GaN (to see the inset of Fig. 1(f)) also shows the characteristic of layered microstrucutre. EDX measurements were carried out to determine the element concentration, and the element ratios were determined as Cr: Ga = 1.96: 1 (to see Fig. 1(e)) and 2.03: 1 (to see Fig. 1(g)) for Cr_2GaC and Cr_2GaN, respectively, which are close to the stoichiometric ratio of 2:1. Here, it is necessary to point out that C and N elements are too light to be exactly detected in Cr_2GaC/N.

Since Z. Liu et al. have reported the magnetic differences between Cr_2GaC and Cr_2GaN [16], we do not show it here. Differently, we focus on the electrical/thermal transport properties of Cr_2GaC and Cr_2GaN. Fig. 2(a) and (b) present the temperature dependence of resistivity $\rho(T)$

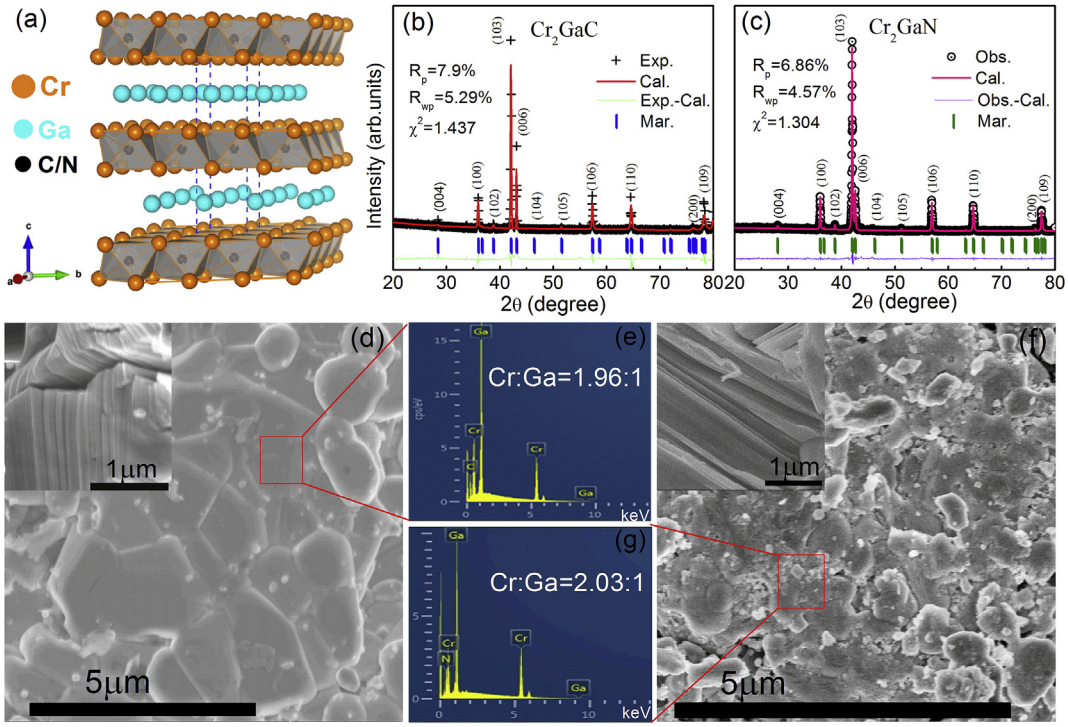

Fig. 1. (Color online) (a) The schematic diagram of crystal structure of Cr_2GaC and Cr_2GaN; The Rietveld refined room-temperature powder XRD pattern for Cr_2GaC (b) and Cr_2GaN (c); (d) FE-SEM images of the Cr_2GaC bulk surface and cross-sectional (the inset); (e) The EDX results for Cr_2GaC; (f) FE-SEM images of the Cr_2GaN bulk surface and cross-sectional (the inset); (g) The EDX results for Cr_2GaN.

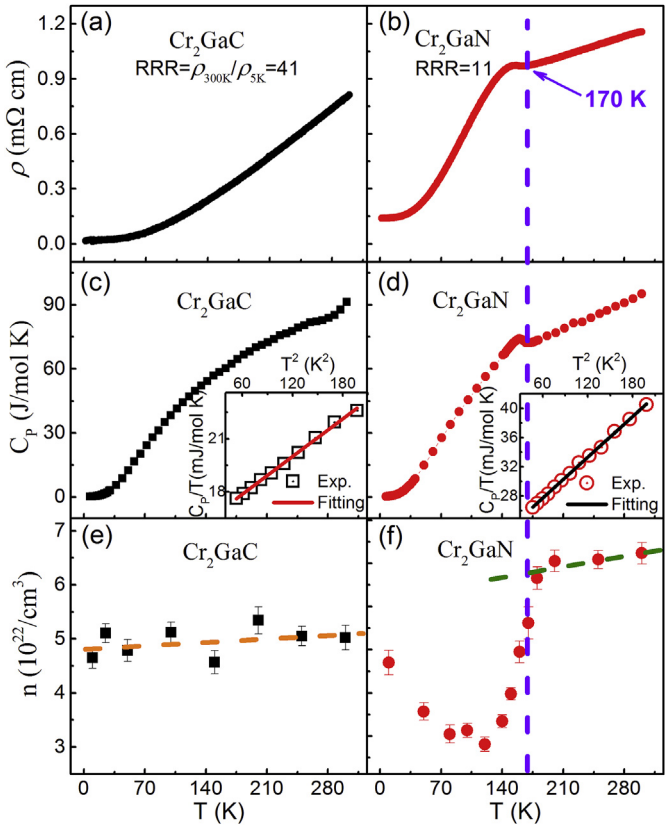

Fig. 2. (Color online) Temperature dependent resistivity (a, b), specific heat (c, d), and density of carriers (e, f) curves between 300 and 5 K for Cr_2GaC and Cr_2GaN; The insets of (c) and (d) show the plot of $C_P(T)/T$ vs T^2 below 20 K for Cr_2GaC and Cr_2GaN, respectively; The dashed lines in (b), (d), (e), and (f) are guide for the eyes.

(300 - 5 K) for Cr_2GaC and Cr_2GaN, respectively. The ρ(T) curve of Cr_2GaC shows a type metallic behavior (to see Fig. 2(a)). The anomalous increase around 170 K, where the SDW appears [16,20], was observed in ρ(T) curve of Cr_2GaN (to see Fig. 2(b)). Besides, the residual resistivity ratio (RRR, defined as RRR = ρ(300K)/ρ(5K)) of Cr_2GaC is much larger than that of Cr_2GaN, indicating a good quality of Cr_2GaC. This is consistent with the surface micrograph results between Cr_2GaC (to see Fig. 1(d)) and Cr_2GaN (to see Fig. 1(f)). Fig. 2(c) and (d) display the temperature dependent specific heat $C_P(T)$ (300 - 5 K) for Cr_2GaC and Cr_2GaN, respectively. The specific heat values of Cr_2GaC and Cr_2GaN at 300 K are 92.2 and 95.1 J/mol K, respectively. Both values are close to the classical Dulong-Petit value C_V = 3NR = 99.7 J/mol K for the specific heat due to acoustic lattice vibrations [23], where N is the number of atom per formula unit and N = 4 for Cr_2GaC/N. This confirms that the compositions of our samples (Cr_2GaC and Cr_2GaN) are very close to the nominal composition, that is to say, C or N defect is very few for our samples. As the temperature falls, the C_P of Cr_2GaC decreases monotonically, while the C_P of Cr_2GaN undergoes an unusual increase around 170 K. The insets of Fig. 2(c) and (d) show the low-temperature specific heat $C_P(T)$ of Cr_2GaC and Cr_2GaN, respectively, plotted as $C_P(T)/T$ vs. T^2. These low-temperature specific heat $C_P(T)$ data can be well expressed via the following equation [24]:

$$C_P(T)/T = \gamma + \beta T^2, \quad (1)$$

where γ stands for the electron specific heat coefficient (Sommerfeld constant), β is phonon specific heat coefficient. According to Eq. (1), the fitted values of γ are 15.74(1) and 22.11(2) mJ/mol K^2 for Cr_2GaC and Cr_2GaN, respectively. In general, Sommerfeld constant γ has a close relationship with density of state around Fermi level [$D(E_F)$] in metallic MAX-phase system [25], namely $\gamma = \pi^2 N_A k_B^2 D(E_F)/3$. Based on the value of γ, we reckoned the $D(E_F)$ via the following formula [26]:

$$D(E_F) = 3\gamma/\pi^2 N_A k_B^2, \quad (2)$$

where N_A is Avogadro constant and k_B is Boltzmann constant. As a result, the $D(E_F)$ of Cr_2GaC and Cr_2GaN are 6.67 and 9.37 sates/eV per unit cell, which are close to the theoretical values (7.5 sates/eV per unit cell for Cr_2GaC and 8.98 sates/eV per unit cell for Cr_2GaN) based on the first-principle calculation [16,18,19]. This indicates that our samples Cr_2GaC and Cr_2GaN are high quality. Fig. 2(e) and (f) reveal the temperature dependent density of carriers $n_D(T)$ between 300 and 5 K for Cr_2GaC and Cr_2GaN, respectively. The temperature dependent n_D were calculated by the formula of $n_D = 1/eR_H$ after measuring the Hall coefficient R_H. As shown in Fig. 2(e) and (f), $n_D(T)$ shows a linear decrease for Cr_2GaC but an abrupt decrease appears at 170 K for Cr_2GaN with decreasing temperature. As mentioned above, all the ρ(T), $C_P(T)$, and $n_D(T)$ curves of Cr_2GaN show an anomalous behavior around 170 K, while Cr_2GaC do not show any anomalous behaviors. As the crystal structure determines the physical properties, we investigated the temperature dependent crystal structure for both Cr_2GaN and Cr_2GaC.

Fig. 3(a) shows the powder XRD patterns for Cr_2GaN between 300 and 35 K. Here, a small amount of Cu powders were added for temperature calibration. There is no structural phase transition over the temperature range of 300–35 K. As shown in Fig. 3(b), the enlargement of XRD pattern near the peaks of (103) and (006) are plotted. As the temperature decreases, the central position of peak (103) shifts to higher angles monotonically, while the central position of peak (006) shifts to higher angles firstly (300 - 170 K) and then moves toward to lower angles (below 170 K). For comparison, we also measured the powder XRD patterns of Cr_2GaC between 300 and 35 K, which were plotted in Fig. 4(a) and (b). Similarly, there is no structural phase transition in Cr_2GaC between 300 and 35 K (to see Fig. 4(a)). As the temperature decreases, both the central positions of peaks (103) and (006) shift to higher angles monotonically (to see Fig. 4(b)).

Subsequently, we refined the lattice constants a and c for both Cr_2GaC and Cr_2GaN at different temperatures by using the Rietveld refinement, which were plotted in Fig. 5(a) and (b). As the temperature falls, the a value decreases monotonically for both Cr_2GaC and Cr_2GaN (to see Fig. 5(a)). As presented in Fig. 5(b), the c value of Cr_2GaC decreases linearly over the measured temperature range, which is consistent with the shift of peak (006) in Fig. 4(b). However, the c value of Cr_2GaN decreases firstly and then shows a sharp increase around 170 K, which is consistent with the shift of peak (006) in Fig. 3(b). Based on the data of a and c, the temperature dependence of c/a and volume V were calculated and were plotted in Fig. 5(c) and (d), respectively. As the temperature falls, the c/a ratio of Cr_2GaC tends to remain unchanged, while the c/a ratio of Cr_2GaN undergoes an abrupt increase at 170 K. The V values of both Cr_2GaC and Cr_2GaN decrease monotonically with decreasing temperature (see Fig. 5(d)). Hereto, the major factor, which leads to the huge difference of physical properti between Cr_2GaC and Cr_2GaN (to see Fig. 2(a)-2(f)), is the anomalous increase of c/a in Cr_2GaN.

As reported by Z. Liu et al., Cr-3d bands dominate $D(E_F)$ and there exists two-dimensional electronic structure (cylindrical shape of Fermi surfaces) in both Cr_2GaC and Cr_2GaN [16]. Why SDW only happens in Cr_2GaN, and even why it appears around 170 K? Furthermore, there also exists an abrupt change in crystal structure (c and c/a) and physical properties (ρ, C_P, and n_D) around 170 K mentioned above in Cr_2GaN. We believe it is not just a coincidence, there must be a certain inner relation between anomalous structure change and physical properties in Cr_2GaN. As we know, the c/a value can qualitatively determine the magnitude of structural anisotropy in layered compounds [27,28]. Here, in layered MAX-phase Cr_2GaN, the lattice constant a decreases while c increases around 170 K gives rise to the anomalous increase of c/a, leading to an enhancement of localization of Cr_2N planes (see

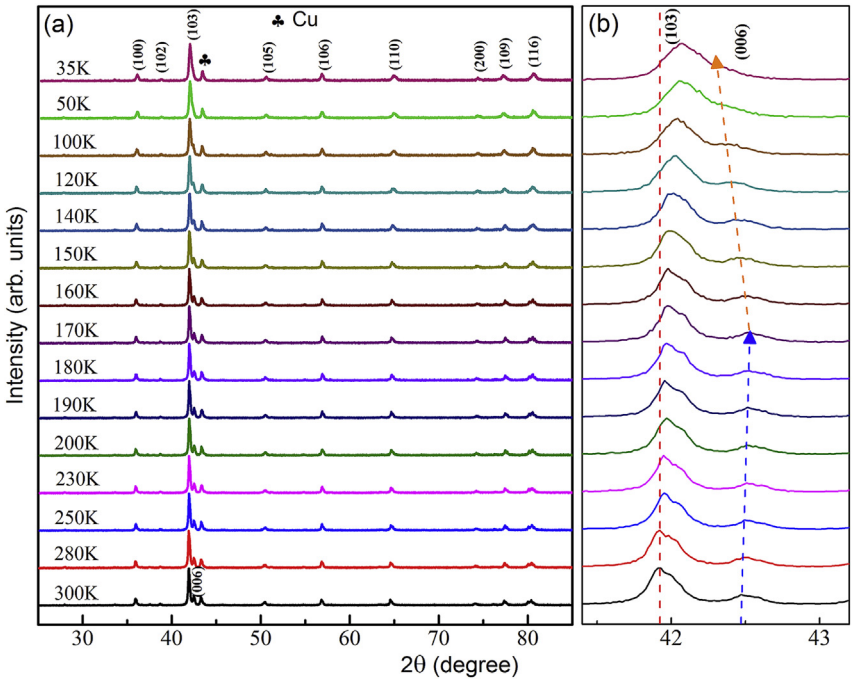

Fig. 3. (Color online) (a) The variable temperature powder XRD patterns between 300 and 35 K for Cr_2GaN; The symbol of club stands for the diffraction peak of Cu powders for calibration purpose; (b) The enlargements of XRD pattern near the peaks of (103) and (006) for Cr_2GaN; The dashed line and dotted line with arrow are guide for the eyes.

Fig. 6). Since the N atom mediates the electron transfer between Cr atoms in Cr_2N planes, the enhancement of localization of Cr_2N planes causes more Cr-3*d* electrons confinement in the Cr_2N planes. This further facilitates the reconstruction of $D(E_F)$ and even the Fermi-surface nesting, resulting in the occurrence of SDW and anomalous changes in resistivity, specific heat, and density of carries around 170 K in Cr_2GaN. Consistent with this argument, some Ge partially substituting Ga sites in Cr_2GaN reduces the c/a ratio, and also suppresses the SDW transition [20]. However, as shown in Fig. 6, there is no anomalous structure change in Cr_2GaC. correspondingly, there is no anomalous change in physical properties. Therefore, the biggest difference between Cr_2GaC and Cr_2GaN is just an anomalous structure change of Cr_2GaN.

4. Conclusion

In summary, we have successfully obtained high quality MAX-phase compounds Cr_2GaC and Cr_2GaN confirmed by the characterizations of XRD, SEM, EDX, RRR. There is a considerable difference between them in resistivity, specific heat, and density of carriers curves around 170 K. After the measurements of the varied temperature XRD for both Cr_2GaC and Cr_2GaN, an abnormal increase of c/a was observed around 170 K in Cr_2GaN. In layered MAX-phase Cr_2GaN, the anomalous increase of c/a ratio enhances the localization of Cr_2N planes and more Cr-3*d* electrons were restricted in Cr_2N planes, resulting in the reconstruction of $D(E_F)$ and even the formation of Fermi-surface nesting. For metallic Cr_2GaN, the reconstruction of $D(E_F)$ causes the occurrences of SDW transition as well as anomalous changes in $\rho(T)$, $C_P(T)$, and $n_D(T)$ curves around

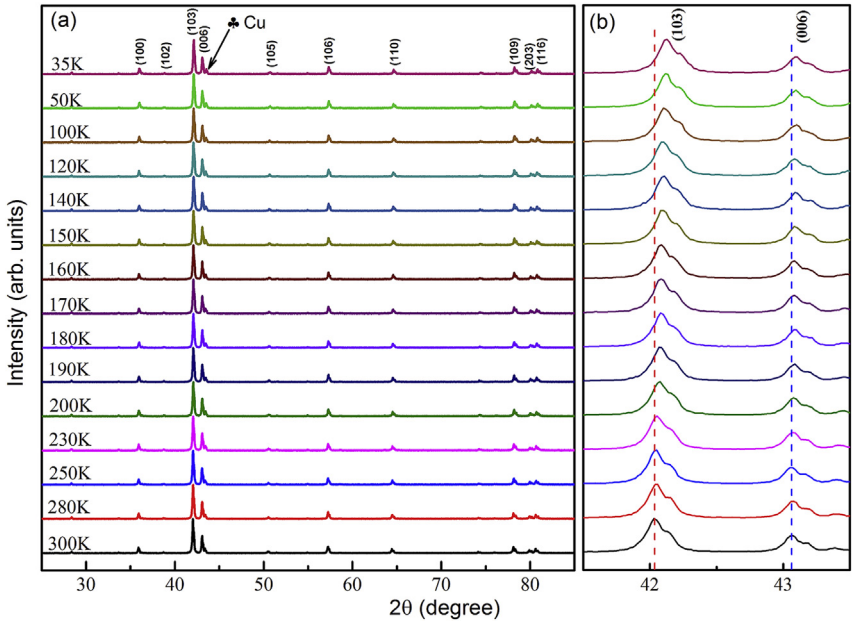

Fig. 4. (Color online) (a) The variable temperature powder XRD patterns between 300 and 35 K for Cr_2GaC; The symbol of club stands for the diffraction peak of Cu powders for calibration purpose; (b) The enlargements of XRD pattern near the peaks of (103) and (006) for Cr_2GaC; The dashed lines are guide for the eyes.

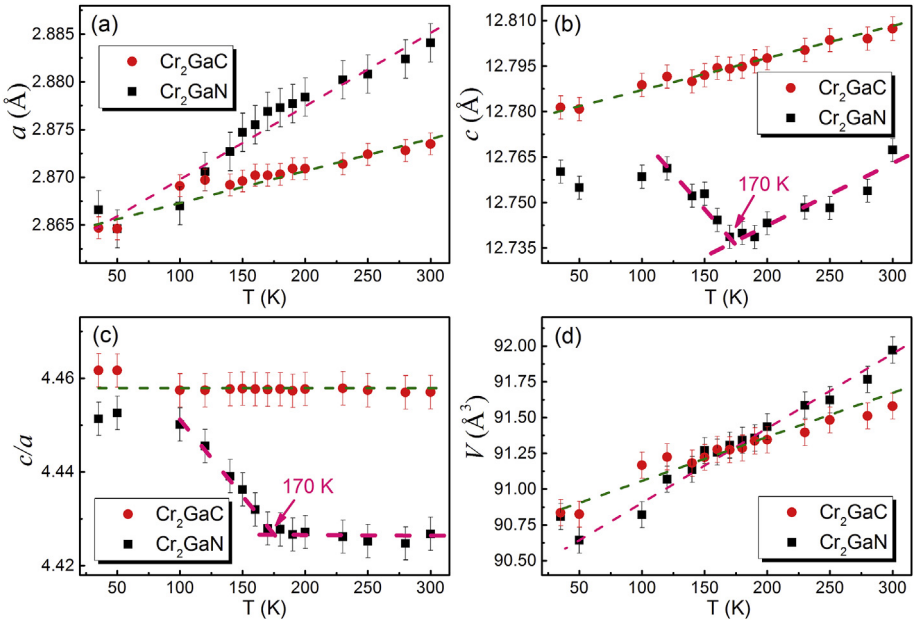

Fig. 5. (Color online) (a)–(d) Temperature dependent lattice constants a, c, c/a, and volume V for Cr_2GaC and Cr_2GaN; The dashed lines are guide for the eyes.

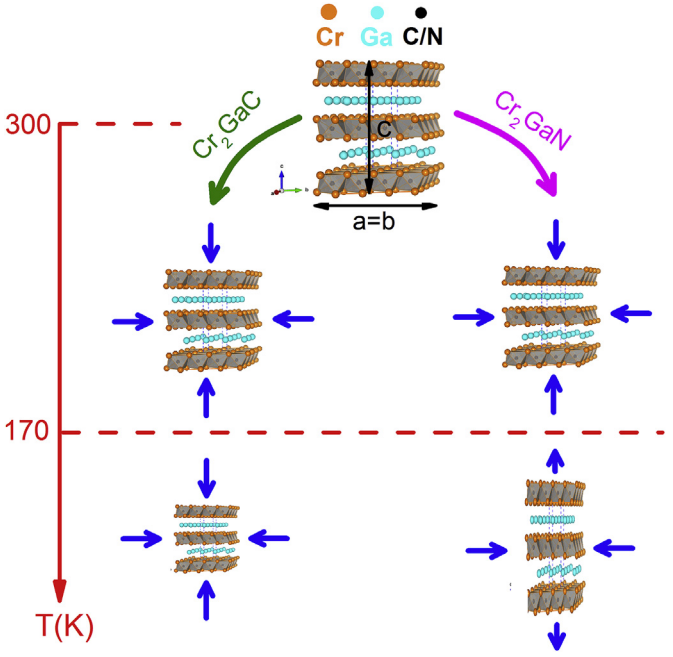

Fig. 6. (Color online) The sketch map of evolution of crystal structure change with temperature for Cr_2GaC and Cr_2GaN.

170 K.

Acknowledgments

This work was supported by the Key Research Program of Frontier Sciences, CAS (QYZDB-SSW-SLH015), National Natural Science Foundation of China under contract Nos. U1632158 and 51322105, Natural Science Foundation of Anhui Province (Grant 1608085QE107). Additionally, this work was also supported by the Youth Innovation Promotion Association of CAS (Grant 2014283).

References

[1] H. Nowotony, Prog. Solid State Chem. 2 (1970) 27–70.
[2] H.J. Yang, Y.T. Pei, J. Th. M. De Hosson, Scripta Mater. 69 (2013) 203–206.
[3] N.A. Phatak, S.K. Saxena, Y.W. Fei, J.Z. Hu, J. Alloy. Comp. 475 (2009) 629–634.
[4] M.W. Barsoum, D. Brodkin, T. El-Raghy, Scripta Mater. 36 (1997) 535–541.
[5] R. Pampuch, J. Lis, L. Stobierski, M. Tymkiewicz, J. Eur. Ceram. Soc. 5 (1989) 283–287.
[6] M.W. Barsoum, L. Farber, I. Levin, A. Procopio, T. El-Raghy, A. Berner, J. Am. Ceram. Soc. 82 (1999) 2545–2547.
[7] B. Manoun, S. Kulkarni, N. Pathak, S.K. Saxena, S. Amini, M.W. Barsoum, J. Alloy. Comp. 505 (2010) 328–331.
[8] N. Tzenov, M.W. Barsoum, J. Am. Ceram. Soc. 83 (2000) 825–832.
[9] M.W. Barsoum, H.-I. Yoo, I.K. Polushina, V. Yu Rud, Yu V. Rud, T. El-Raghy, Phys. Rev. B 62 (2000) 10194.
[10] H.-I. Yoo, M.W. Barsoum, T. El-Raghy, Nature (London) 407 (2000) 581–582.
[11] Z. Liu, K. Takao, T. Waki, Y. Tabata, H. Nakamura, J. Phys. Conf. Series 868 (2017) 012016.
[12] C.M. Hamm, J.D. Bocarsly, G. Seward, U.I. Kramm, C.S. Birkel, J. Mater. Chem. C 5 (2017) 5700–5708.
[13] S. Lin, P. Tong, B.S. Wang, Y.N. Huang, W.J. Lu, D.F. Shao, B.C. Zhao, W.H. Song, Y.P. Sun, J. Appl. Phys. 113 (2013) 053502.
[14] Q.Z. Tao, C.F. Hu, S. Lin, H.B. Zhang, F.Z. Li, D. Qu, M.L. Wu, Y.P. Sun, Y. Sakka, M.W. Barsoum, Mater. Res. Lett. 2 (2014) 192–198.
[15] A.S. Ingason, A. Mockute, M. Dahlqvist, F. Magnus, S. Olafsson, U.B. Arnalds, B. Alling, I.A. Abrikosov, B. Hjörvasson, P.O.Å. Persson, J. Rosen, Phys. Rev. Lett. 110 (2013) 195502.
[16] Z. Liu, T. Waki, Y. Tabata, K. Yuge, H. Nakamura, I. Watanabe, Phys. Rev. B 88 (2013) 134401.
[17] M.W. Barsoum, L. Farber, Science 284 (1999) 937–939.
[18] A. Bouhemadou, Solid State Sci. 11 (2009) 1875–1881.
[19] Z.J. Yang, R.F. Linghu, X.L. Cheng, X.D. Yang, Acta Phys. Sin. 61 (2012) 046301.
[20] Y.F. Li, J.Z. Liu, W.H. Liu, X.Y. Zhu, H.H. Wen, Philos. Mag. 95 (2015) 2831–2837.
[21] K. Momma, F. Izumi, J. Appl. Crystallogr. 44 (2011) 1272–1276.
[22] C.F. Hu, L.F. He, M.Y. Liu, X.H. Wang, J.Y. Wang, M.S. Li, Y.W. Bao, Y.C. Zhou, J. Am. Ceram. Soc. 91 (2008) 4029–4035.
[23] R.J. Goetsch, V.K. Anand, A. Pandey, D.C. Johnston, Phys. Rev. B 85 (2012) 054517.
[24] P. Tong, Y.P. Sun, X.B. Zhu, W.H. Song, Phys. Rev. B 73 (2006) 245106.
[25] S. Lin, Y.N. Huang, L. Zu, X.C. Kan, J.C. Lin, W.H. Song, P. Tong, X.B. Zhu, Y.P. Sun, J. Alloy. Comp. 680 (2016) 452–461.
[26] L. Schoop, M. Hirschberger, J. Tao, C. Felser, N.P. Ong, R.J. Cava, Phys. Rev. B 89 (2014) 224417.
[27] H.I. Faraoun, F.Z. Abderrahim, C. Esling, Comput. Mater. Sci. 74 (2013) 40–49.
[28] M. Khazaei, M. Arai, T. Sasaki, M. Estili, Y. Sakka, Sci. Technol. Adv. Mater. 15 (2014) 014208.